Proceedings of the
Annual Stability Conference
Structural Stability Research Council
Atlanta, Georgia, April 21-24, 2026

Experimental investigation of torsional-flexural response of intermediately stiffened lipped channels cold-formed from 690 MPa (100 ksi) steel

Damir Akchurin[1], Fidence Cyizere Rukundo[2], Stanley Zhang[3], Shahabeddin Torabian[4, 5], Sándor Ádány[6, 7], Benjamin W. Schafer[8]

Abstract

The main objective of this study is to provide a brief summary of recent torsional-flexural tests conducted on a lipped channel section featuring multiple intermediate longitudinal stiffeners in the web and flanges, as well as return lips. The specimens were cold-formed from high-strength low-alloy steel with a nominal yield strength of 690 MPa (100 ksi). These torsional-flexural tests extend previously conducted pure compression and flexural tests on the same section and are intended to assess the adequacy of current design strength prediction equations for cold-formed steel members fabricated from high-strength steels under different loading conditions. Two experimental test configurations were explored: (1) a 3-point bending setup with warping restrained supports, and (2) a 4-point bending setup with warping unrestrained supports. The advantages and limitations of each configuration are discussed. Overall, the second configuration provides a more straightforward approach for conducting torsional-flexural tests on cold-formed steel sections and is better suited for computational modeling due to boundary conditions that more closely approximate idealized behavior. A brief discussion of the preliminary experimental and numerical results is provided. These results will be used to evaluate the adequacy of the design strength prediction equations provided in the AISI S100-2024 Specification.

[1]Graduate Research Assistant, Department of Civil and Systems Engineering, Johns Hopkins University, Baltimore, MD, USA, akchurd1@jhu.edu
[2]Graduate Research Assistant, Department of Civil and Systems Engineering, Johns Hopkins University, Baltimore, MD, USA, fcyizer1@jhu.edu
[3]Undergraduate Research Assistant, Department of Civil and Mechanical Engineering, State University of New York Polytechnic Institute, Utica, NY, USA, zhangsh1@sunypoly.edu
[4]Associate Research Scientist, Department of Civil and Systems Engineering, Johns Hopkins University, Baltimore, MD, USA, torabian@jhu.edu
[5]Senior Project Manager, Simpson Gumpertz & Heger, Washington, DC, USA, storabian@sgh.com
[6]Associate Research Scientist, Department of Civil and Systems Engineering, Johns Hopkins University, Baltimore, MD, USA, asandor2@jhu.edu
[7]Professor, Department of Structural Mechanics, Budapest University of Technology and Economics, Budapest Hungary, adany.sandor@emk.bme.hu
[8]Professor, Department of Civil and Systems Engineering, Johns Hopkins University, Baltimore, MD, USA, schafer@jhu.edu

1. Introduction

For the past 70 years, particularly in the United States, the structural cold-formed steel (CFS) market has predominantly featured relatively simple C-, U-, and Z-sections. However, more cost-effective manufacturing tooling, combined with advancements in material science and generalized design methods, have spurred the demand for and proliferation of more complex and better-performing CFS sections, which commonly incorporate stiffening features like intermediate stiffeners and return lips (Akchurin et al., 2024; Ding, 2022).

The experimental study presented herein investigates the torsional-flexural response behavior of a cold-formed lipped channel section with intermediate stiffeners and return lips roll-formed from high-strength low-alloy (HSLA) steel with a nominal yield strength of 690 MPa (100 ksi). One of the main intended commercial applications for the studied section is as driven piles for ground-supported solar panel array installations. Earlier studies by the authors have explored the pure compressive (Akchurin et al., 2023a, 2023b, 2024) and flexural (Rukundo et al., 2025) responses of the studied section, and, in this study, torsional-flexural response, which is most likely to dominate the design of such driven piles, is investigated.

This study examines two experimental configurations for evaluating the torsional-flexural strength of the studied section: (1) a 3-point bending setup with warping-restrained supports, and (2) a newly developed 4-point bending setup with warping-free supports. The respective advantages and limitations of the two configurations are discussed. The experimental findings indicate that the second configuration offers a more practical and mechanically consistent framework for torsional-flexural testing of cold-formed steel members and is better suited for numerical modeling due to boundary conditions that more closely represent idealized behavior. Finally, preliminary experimental results obtained using this configuration are presented and discussed.

2. Nominal Section

The nominal section studied herein was developed by a commercial supplier as a prototype. The nominal section features a 152.4 mm (6 in.)-wide and 101.6 mm (4 in.)-deep lipped channel section as shown in Figure 1. The nominal section features several intermediate stiffening elements: two hat-shaped stiffeners in the web, one stiffener in each flange, edge stiffeners, and return lips on the edge stiffeners. The nominal thickness of the section is 1.9 mm (0.075 in.).

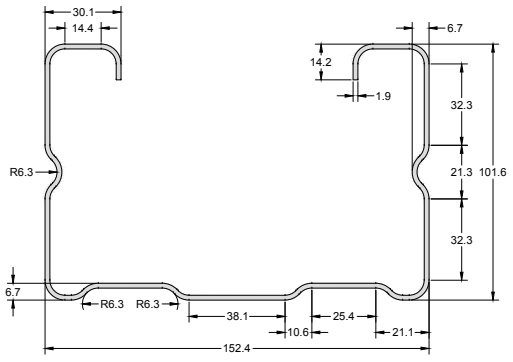

Figure 1: Nominal dimensions (mm) of the studied section. All inner radii are 6.0 mm unless noted otherwise.

3. Test Setups

3.1. Test Setup #1

Test Setup #1, shown in Figure 2, employed a single collar fabricated from 152.4 mm (6 in.)-wide and 12.7 mm (½ in.)-thick hollow square steel (HSS) section, bolted at the midspan of 3.7 m (12 ft)-long specimens to apply combined torsional-flexural loading. A variation of this HSS collar setup was productively used previously in flexural testing (Rukundo et al., 2025). Loading was introduced eccentrically through an adjustable loading eccentricity e measured from the section shear center by adjusting the location of connection between the actuator and moment arm. At the supports, CFS track sections were fastened to the test specimen to restrain warping by locally increasing the Saint-Venant torsional constant J. In addition, twist at the supports was further restrained using a pair of 152.4 mm (6 in.)-wide angles, while 12.7 mm (½ in.)-diameter rollers placed under the specimen allowed flexural rotation. Displacements and rotations resulting from combined torsional-flexural loading were measured using position transducers located at the quarter points along the specimen length and on the moment arm.

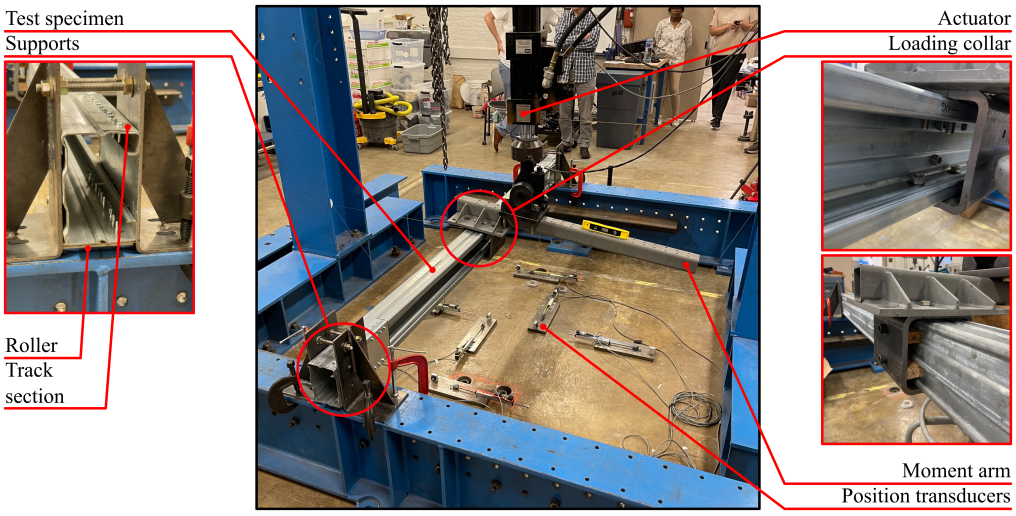

Figure 2: Test setup #1.

Although this configuration allowed controlled application of combined torsional-flexural loading, it had several notable limitations. First, the imposed warping restraint at the supports does not reflect typical boundary conditions of CFS steel members in practice, where warping is generally unrestrained. Second, the combined warping and twist restraints significantly complicate numerical modeling, as accurate representation of the boundary conditions requires explicit modeling of both torsional and warping stiffness at the supports, and potentially even modeling the specific screws and details in which the end warping restraint is augmented. Finally, the restrained warping conditions hinder isolation of torsional stress resultants, since the measured response reflects coupled contributions from flexure M_{xx}, Saint-Venant torsion T_{sv}, and warping torsion T_w.

3.2. Test Setup #2

To address these limitations, test setup #2, shown in Figure 3, was developed to provide a more direct representation of torsional-flexural behavior of CFS members while isolating the fully warping unrestrained behavior simplifying further investigations. This setup employed 1.8 m (6

ft)-long specimens and a series of custom-made collars in which the exact cross-section was machined out of 12.7 mm (½ in.)-thick aluminum plates. The loading collars were designed to apply torsional loading uniformly around the cross section while permitting free warping of the test specimen, thereby allowing the response to be dominated by warping torsion T_w. Similar collars were used at the supports to ensure consistent boundary conditions along the specimen length. At the supports, the bottoms of the collars were rounded to allow flexural rotations, effectively approximating pinned boundary conditions in flexure. In addition, angles of twist were measured directly using inclinometers mounted on the actuator and moment arm, eliminating the need to back-calculate torsional rotations from displacement measurements, as was required in test setup #1. This direct measurement improved the accuracy of torsional response characterization and simplified interpretation of the experimental results.

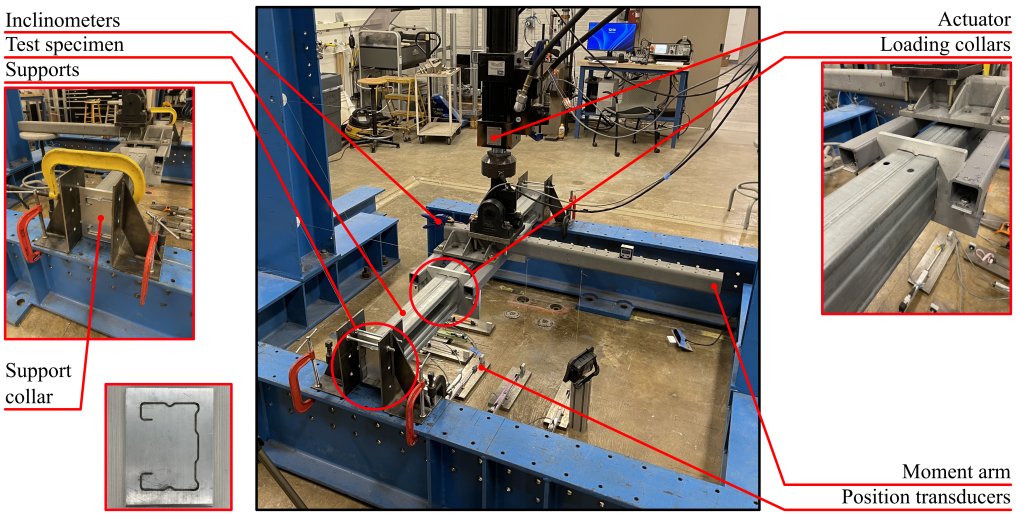

Figure 3: Test setup #2.

Unlike test setup #1, no intentional warping restraint were introduced at the supports, resulting in boundary conditions that more closely resemble those encountered by CFS members in typical construction. This configuration offers several key advantages. First, by allowing unrestrained warping and avoiding localized torsional restraint at the supports, test setup #2 enables clearer separation and interpretation of torsional stress resultants and deformation components. Second, the simplified and well-defined boundary conditions significantly facilitate analytical predictions and related numerical modeling. Finally, a key advantage of this configuration is the creation of a region of constant flexural moment M_{xx} and bimoment B at midspan between the loading collars as shown in Figure 4, enabling direct evaluation of torsional-flexural strength for open thin-walled sections where bimoment B dominates the torsional response, using well-defined internal force distributions. Consequently, test setup #2 is better suited for direct comparison with numerical simulations and further assessment of the adequacy of existing design strength prediction equations in the AISI S100-2024 Specification.

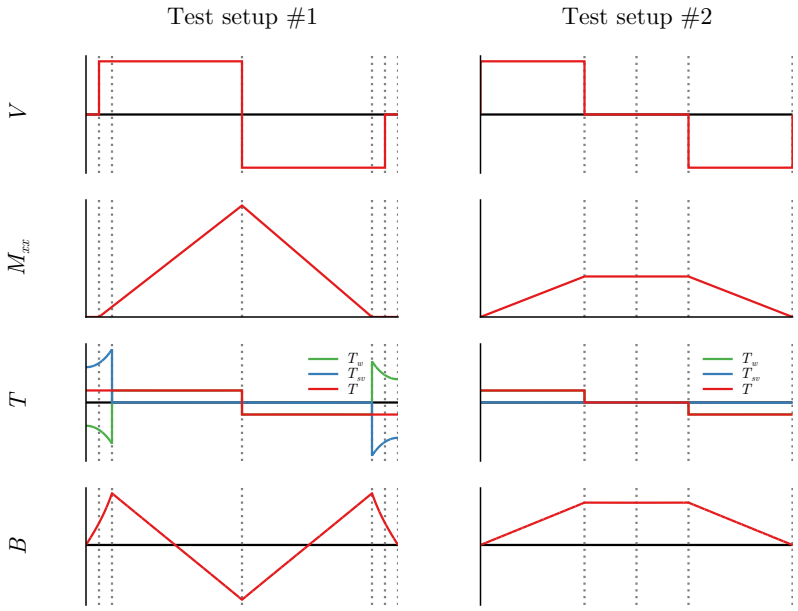

Figure 4: Comparison of shear V, moment M_{xx}, torsion T (warping T_w and Saint-Venant T_{sv} torsions included), and bimoment B diagrams for test setups #1 and #2.

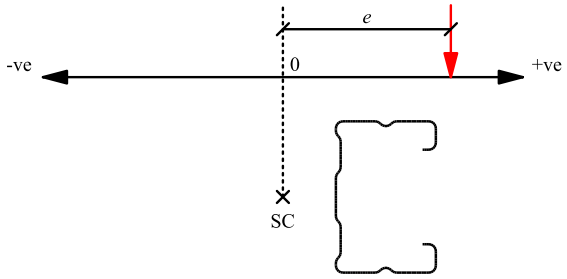

Sign convention for loading eccentricity e

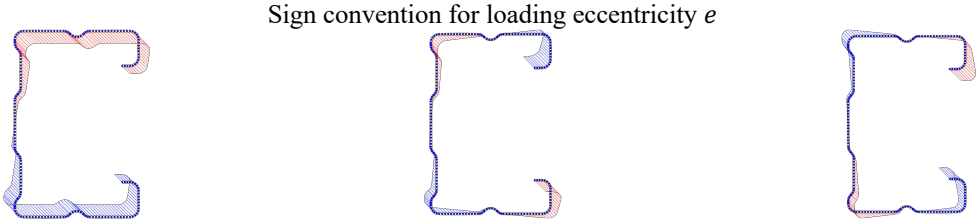

σ_b due to M_{xx} σ_w due to B (+ve e) σ_w due to B (-ve e)

Figure 5: Sign convention for loading eccentricity e and associated longitudinal stress distributions due to moment M_{xx} and bimoment B.

Lastly, it is noted that both test setups allow a wide range of loading eccentricities e measured from the shear center of the studied section, and, therefore, allow to study a wide range of torsion-to-flexure interaction by adjusting the connection location between the actuator and the moment arm. Following the sign convention adopted in this study, illustrated in Figure 5, positive values of e correspond to loading scenarios in which the bimoment B results in compressive longitudinal warping stresses σ_w in the return lip of the bottom flange, which are partially counteracted by tensile longitudinal bending stresses σ_b resulting from moment M_{xx}. Conversely, negative values

of e correspond to loading scenarios in which the bimoment B results in compressive longitudinal warping stresses σ_w in the return lip of the top flange, which are further amplified by compressive longitudinal bending stresses σ_b resulting from moment M_{xx}.

4. Numerical Modeling

The specimens tested using test setup #2 were modeled using a preliminary finite element model developed using Abaqus shown in Figure 6. The material behavior was modelled using nonlinear elastic-plastic constitutive model based on companion coupon tests with the yield strength F_y of 101.4 ksi and ultimate strength F_u of 109.4 ksi (Rukundo et al., 2025). Boundary conditions were applied to reproduce the experimental setup. The support collars at the supports were represented by restraining transverse displacements of the sections while allowing free longitudinal sliding; rotation about the longitudinal axis was restrained by fixing the rotational degree of freedom. At the two load application locations, the sections were coupled to a reference point RP3, representing the loading point of the actuator, in all translational and rotational degrees of freedom except for the longitudinal displacement, which was left unconstrained. This coupling ensured uniform transfer of torsional deformation across the section and allowed warping along the length of the specimen. To prevent rigid-body motion while preserving the torsional response, the longitudinal displacement at the beam midspan was constrained.

The actuator was represented in the numerical model using a deformable wire element, created to match the length of the actuator used in the tests. The actuator was assigned an isotropic elastic material with a prescribed coefficient of thermal expansion, which was used to impose artificial thermal strain rather than to represent a physical thermal condition. A circular section was defined and assigned to the actuator's wire element. Boundary conditions were defined to replicate the actuator kinematics observed in the test: the top of the actuator was fixed in all translational degrees of freedom and in rotations about the transverse axes, while rotation about the longitudinal axis of the test specimen was left free; the bottom end of the actuator was coupled to the reference point RP3 in translation, while all rotational degrees of freedom were left unconstrained. Loading was introduced as a simulated displacement of the actuator through a predefined, spatially uniform temperature field applied to the actuator elements and held constant over the actuator region. Through the assigned coefficient of thermal expansion, the imposed temperature changes generated artificial thermal strain, which induced controlled actuator deformation and, through the kinematic coupling at RP3, produced torsional rotation of the specimen. This approach provided a smooth, force-consistent representation of the experimental actuator while avoiding the numerical difficulties associated with movement of the actuator observed during testing. The analysis was performed using a nonlinear static procedure, and no initial geometric imperfections were included in these preliminary analyses.

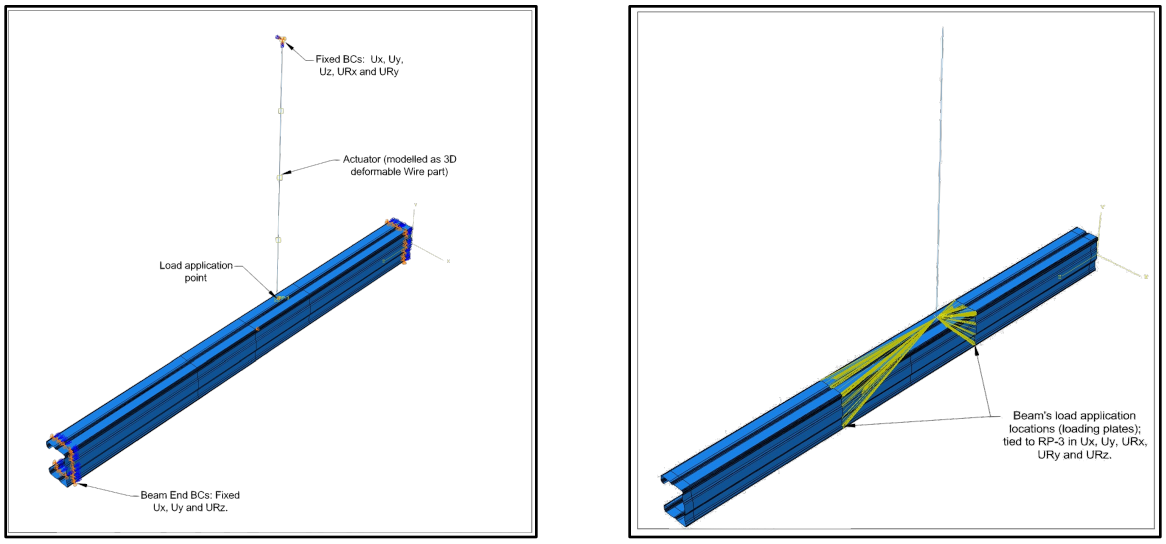

(a) (b)

Figure 6: Finite element model of a test specimen showing boundary conditions and actuator idealizations: (a) boundary conditions and (b) kinematic coupling.

5. Preliminary Test Results and Discussion

5.1. Comparison of Test Setups

To illustrate the experimental responses obtained using the two test setups, a comparison of the torsion-to-twist T-ϕ curves for two specimens tested with the same loading eccentricity e of +203.2 mm (+8 in.), is presented in Figure 7. The applied torsion T is intentionally normalized by E/L_t^3, where L_t is the torsion span length, equal to 1.8 m (6 ft) for test setup #1 and 0.6 m (2 ft) for test setup #2. Under the assumption that the response is dominated by warping torsion, this normalization yields an initial slope of the T-ϕ curves, a measure of effective warping stiffness, that is directly comparable to the nominal warping stiffness C_w, which is calculated as 1.143×10^{-7} mm^6 (30.7 in.^{6}) for the nominal section.

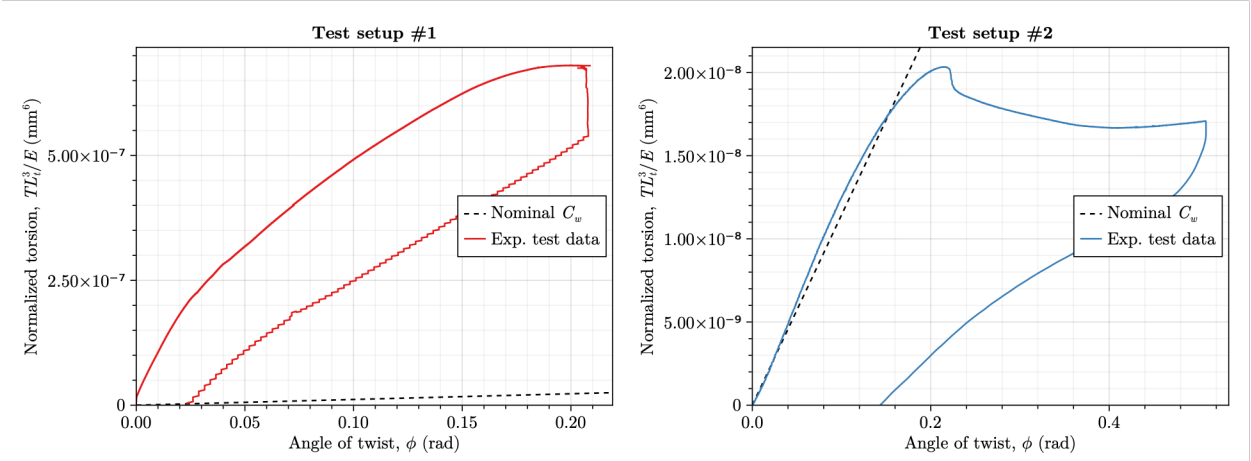

Figure 7: Comparison of the experimental responses obtained using the two test setups.

As shown in Figure 7, the effective warping stiffness for the specimen tested using test setup #2 is 1.072×10^{-7} mm^6 (28.8 in.^{6}) and closely agrees with the nominal C_w. In contrast, the specimen tested using test setup #1 has the effective warping stiffness of 94.684×10^{-7} mm^6 (2542.6 in.^{6}), two

orders of magnitude larger than the nominal C_w. This difference indicates that the track sections fastened at the supports in test setup #1 introduce significant Saint-Venant torsion T_{sv} at the supports, thereby suppressing warping deformation and fundamentally changing the experimental torsional response. As a result, the measured behavior in test setup #1 reflects an expected coupled response dominated by Saint-Venant torsion T_{sv} rather than the intended warping torsion T_w as evident from torsion diagram shown in Figure 4 and observed from significant shear deformations of the studied section at the supports shown in Figure 8.

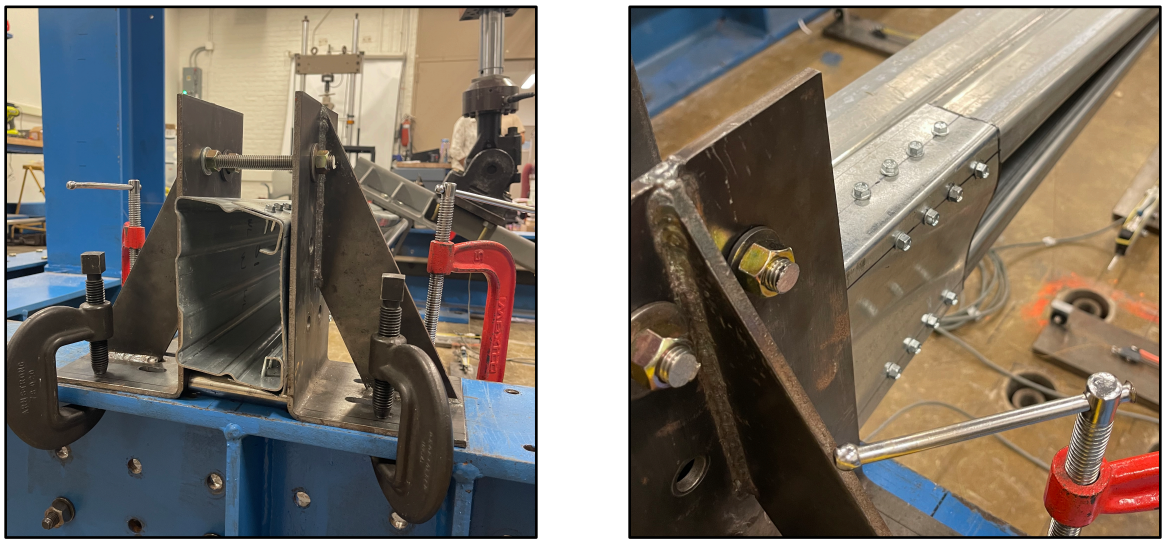

Figure 8: Observed shear deformations of the studied section at the supports of test setup #1.

Additionally, by allowing free warping and minimizing unintended warping restraint, test setup #2 produces a torsional response consistent with Vlasov theory for open thin-walled sections. This not only facilitates direct computation of the bimoment $B = TL_s$ from the applied torsion $T = Pe/2$, where L_s is the shear span length, but also significantly simplifies numerical modeling by enabling well-defined boundary conditions. As a result, test setup #2 is better suited for validating analytical and numerical models and for assessing torsional-flexural strength predictions for CFS members.

5.2. Comparison of Test Results Against Numerical Models

Confirming that the novel test setup #2 provides a clear path towards torsional-flexural testing of CFS members, two specimens with large loading eccentricities e of -304.8 mm (-12 in.) and +304.8 mm (+12 in.) were tested using test setup #2 and the results were compared to the finite element models discussed earlier. The comparison between the resulting actuator loads P and angles of twist ϕ measured at the loading collar locations shown in Figure 9 demonstrated good agreement both in terms of stiffness and ultimate strengths between the experimental and numerical results.

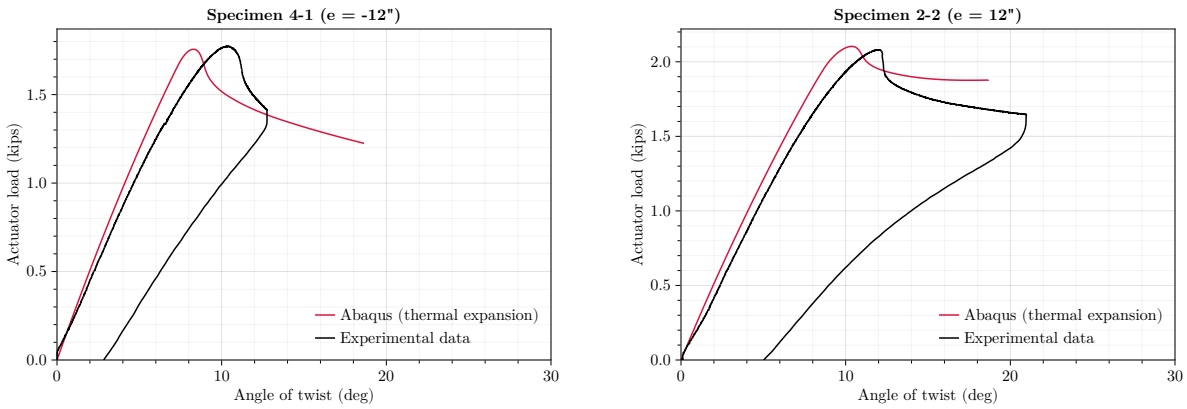

e of -304.8 mm (-12 in.) *e* of +304.8 mm (+12 in.)

Figure 9: Comparison of the experimental test results against the results of numerical modeling for test setup #2.

In both tests, the observed failure modes at peak loads were consistent with the expected distributions of longitudinal stresses for positive and negative values of *e* discussed earlier: test specimen with *e* of -304.8 mm (-12 in.) developed a failure mechanism in the return lip in the top flange and test specimen with *e* of +304.8 mm (+12 in.) developed a failure mechanism in the return lip in the bottom flange. For these specimens, the observed failure modes were primarily governed by material yielding rather than instability phenomena - no local, distortional, or global instability was observed prior to reaching the peak load. Instead, the specimens exhibited a stable, monotonic response up to failure, with strength degradation occurring only after the onset of significant yielding. Although yielding controlled the ultimate capacity, the resulting failures were characterized by spatially distributed plastic mechanisms involving combined bending, torsion, and warping effects. This behavior indicates that the response of the tested section was dominated by cross-sectional yielding under coupled longitudinal flexural and warping stresses. In both tests, the test specimens also exhibited clear warping deformations at the supports, as shown in Figure 11, further confirming the warping-dominated behavior.

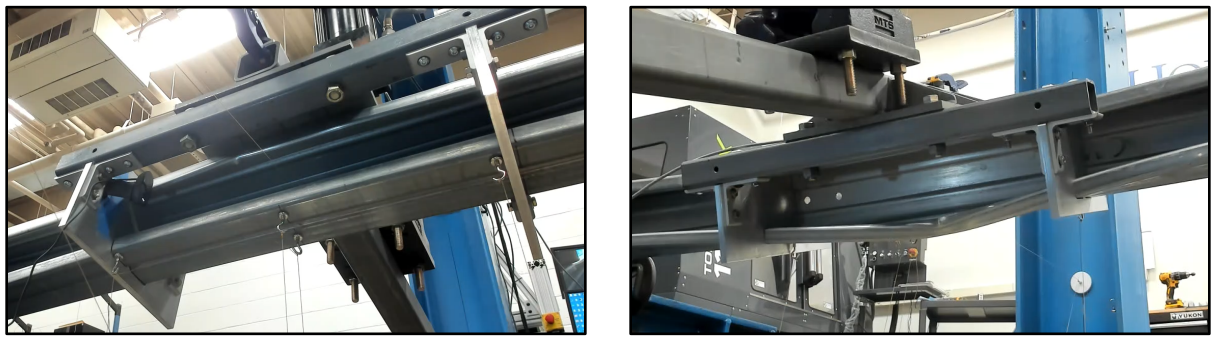

e of -304.8 mm (-12 in.) *e* of +304.8 mm (+12 in.)

Figure 10: Observed failure modes at peak loads.

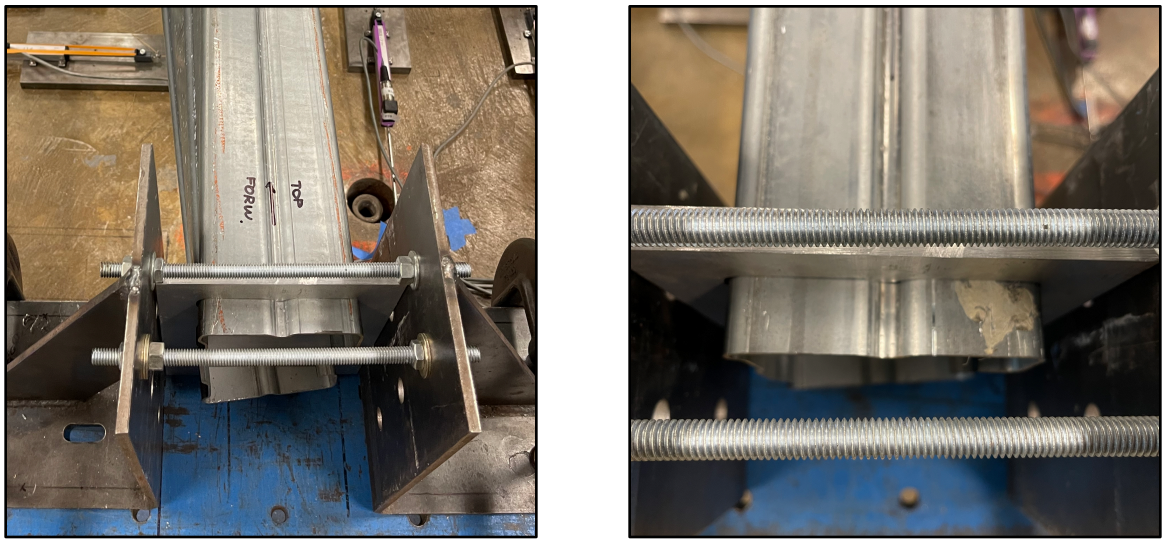

Figure 11: Observed warping deformations at the supports of test setup #2.

6. Conclusion

This study presented a preliminary experimental investigation of the torsional-flexural response of an intermediately stiffened cold-formed steel lipped channel section fabricated from 690 MPa (100 ksi) steel. Two experimental test configurations were examined: a test setup with warping-restrained boundary conditions and a novel setup with warping-unrestrained boundary conditions. The comparison demonstrated that the warping-restrained configuration introduces significant Saint-Venant torsional restraint, resulting in torsional stiffnesses that are inconsistent with theoretical warping behavior for open thin-walled sections. In contrast, the proposed warping-unrestrained test setup produced torsional responses in close agreement with Vlasov theory, enabled direct computation of bimoment, and significantly simplified numerical modeling. The improved boundary conditions also resulted in a well-defined region of constant bending moment and bimoment, making the setup particularly suitable for studying torsional-flexural interaction in cold-formed steel members.

Future work will expand this study to include a comprehensive set of experimental results spanning a wider range of loading eccentricities and torsion-to-flexure ratios. Additional investigations will examine the influence of initial geometric imperfections on torsional-flexural strength and failure modes. The experimental results will be used to assess the adequacy of existing torsional-flexural strength prediction equations in the AISI S100 Specification and to support the development of improved design guidance for cold-formed steel members fabricated from high-strength steels.

Acknowledgements

This material is based upon work supported by the National Science Foundation under grant #2349378 as part of the project “REU Site: Research on Sustainable Energy Technology and Systems (ROSETAS)”. Any opinions, findings and conclusions or recommendations expressed in this material are those of the author(s) and do not necessarily reflect the views of the National Science Foundation. We would like to thank Nucor Corp. for providing the test specimens. We would also like to thank FABCO, a company that expertly fabricated the test specimens. The authors would also thank lab manager Kyle Coleman for providing his technical assistance throughout the testing and skillfully manufacturing the custom collars used in testing.

References

Akchurin, D., Ding, C., Bogh, B., Torabian, S., Schafer, B.W., 2023a. Response and Strength of Intermediately Stiffened Cold-Formed Steel Lipped Channel Columns Formed from 100 ksi (690 MPa) Steel, in: Proceedings of the Annual Stability Conference. Presented at the Annual Stability Conference, Structural Stability Research Council, Charlotte, NC.

Akchurin, D., Torabian, S., Ding, C., Schafer, B.W., 2023b. Compressive Capacity of Cold-Formed Steel High Strength Low-Alloy Lipped Channels with Intermediate Stiffeners (No. R-2023-1). Cold-Formed Steel Research Consortium.

Akchurin, D., Torabian, S., Schafer, B.W., 2024. High-Strength Cold-Formed Steel Stiffened Channel Section: Axial Compressive Strength and Initial Geometric Imperfections. Thin-Walled Structures 112604. https://doi.org/10.1016/j.tws.2024.112604

Ding, C., 2022. Strength and Behavior of Advanced High Strength Steel Structural Components. Johns Hopkins University, Baltimore, MD.

Rukundo, F.C., David, S., Torabian, S., Schafer, B.W., 2025. Flexural Tests on High Strength Cold-Formed Steel Solar Piles, in: Proceedings of the Annual Stability Conference. Presented at the Annual Stability Conference, Structural Stability Research Council, Louisville, KY.